Terahertz pulses generate two types of laser-induced periodic surface structures on phase change material $Ge_2Sb_2Te_5$

You Wei Wang[1] · Zihao Yang[1] · Kosaku Kato[1] · Verdad C. Agulto[1] · Thanh Nhat Khoa Phan[1] · Kotaro Makino[2] · Junji Tominaga[3] · Goro Isoyama[4] · Makoto Nakajima[1]

Abstract

This study investigates the formation of two types of laser-induced periodic surface structures (LIPSS) on amorphous $Ge_2Sb_2Te_5$ (GST) using terahertz free-electron laser (THz-FEL) irradiation. The THz pulses used in this study consist of a macro pulse containing 150 micro pulses, each with a duration of 2 ps. The central wavelength λ of the THz radiation is 75 µm. By exposing GST to THz-FEL pulses at fluences up to 35 J/cm², two distinct periodic structures were observed: low spatial frequency LIPSS (LSFL) and high spatial frequency LIPSS (HSFL). The LSFL formed parallel to the laser's polarization direction with a period of approximately λ/4.5. The HSFL, with a period λ/18, formed perpendicular to the polarization near the ablation edges. The periods of the generated HSFL and LSFL are 4 µm and 16 µm, respectively, and can be observed with an optical microscope. The period of the LSFL is generally consistent with λ/*n* (where *n* is the material's refractive index), which is the approximate value expected based on previous reports in the optical region. This work contributes to a deeper understanding of LIPSS formation mechanisms under long-wavelength terahertz irradiation and suggests pathways for fine-tuned surface structuring applications using THz-FEL.

Keywords LIPSS · GST · Terahertz waves · Free electron laser

1 Introduction

With the invention of the laser, laser-induced periodic surface structures (LIPSS) were discovered decades ago [1]. These periodic structures induced by lasers on metals, semiconductors, and dielectric surfaces have garnered widespread interest. Starting from Sipe's work [2], numerous theories have emerged to explain the formation of LIPSS. The mechanisms are broadly categorized into the theory of reproducing the electromagnetic field distribution and that of self-organized pattern formation [3,4]. In recent years, advances in laser technology, particularly the development of picosecond (ps) and femtosecond (fs) ultrashort pulse lasers, have led to the discovery of an increasing number of LIPSS [5-11]. However, with the emergence of various types of LIPSS, researchers have faced increasing difficulty in explaining their formation through a unified theory. Numerous experimental and theoretical studies have investigated the mechanisms behind LIPSS formation [12-14]. These studies have revealed key physical processes that govern the periodic patterns, including surface plasmon polariton (SPP) excitation [15], parametric decay [16], and second harmonic generation [17]. Previous studies have identified several critical laser parameters that influence the period of LIPSS, including the polarization, wavelength, energy fluence, number of superimposed pulses, and ambient air pressure [18,19]. However, further studies are needed to understand the LIPSS formation mechanism fully.

In recent years, terahertz (THz) technology has made

Makoto Nakajima

nakajima.makoto.ile@osaka-u.ac.jp

[1] Institute of Laser Engineering, The University of Osaka, Suita, Osaka 565-0871, Japan

[2] Semiconductor Frontier Research Center, National Institute of Advanced Industrial Science & Technology (AIST), Tsukuba, Ibaraki, 305-8568 Japan

[3] Device Technology Research Institute, National Institute of Advanced Industrial Science & Technology (AIST), Tsukuba, Ibaraki, 305-8568 Japan

[4] SANKEN (Institute of Scientific and Industrial Research), The University of Osaka, Ibaraki, Osaka, 567-0047, Japan

significant advancements [20,21]. Especially, intense THz free electron laser (FEL) has opened up research in nonlinear optics within the THz domain, such as harmonic generation [22,23] and the reconfiguration of magnetic domain structures [24]. The intense THz-FEL also recently demonstrated forming LIPSS with a micrometer scale [25-28]. Since THz waves have a much longer wavelength (30-3000 μm) and much lower photon energy (0.4–40 meV) than optical waves, the comparative researches between the LIPSS induced with THz waves and those induced with optical waves will be effective to deepen the understanding on the LIPSS formation mechanism. By analyzing the similarities and differences in the periodic structures, formation conditions, and material responses under these two different excitation sources, researchers can gain valuable insights into the physical processes governing LIPSS generation. This includes exploring factors such as energy absorption, thermal effects, electron excitation dynamics, and surface plasmon interactions, which may vary significantly between THz and optical regimes. Such investigations will not only contribute to a more comprehensive theoretical framework for LIPSS formation but also help optimize its applications in areas such as material processing, optical engineering, and nanostructure fabrication. In addition, the LIPSS formed with the THz waves have the advantage that their structures are micrometer-scale and can be observed using an optical microscope, without nanoscale observation instruments such as a scanning electron microscope. This enables us to easily examine their structures in detail and get plenty of information useful for the studies on the LIPSS formation mechanism. In our previous work [25,27], we achieved LIPSS formation on Ge–Sb–Te (GST)-based chalcogenide using THz-FEL irradiation. The chalcogenides are widely used as phase-change materials (PCMs) in optical storage devices like DVDs and Blu-Ray discs, and the detailed investigation of their response to electromagnetic waves is expected to provide insight useful for developing new PCMs. Based on this potential, the properties of GST in the THz domain have been extensively studied in recent years [29-32]. The LIPSS on chalcogenides have been mainly studied using visible or near-infrared lasers [33-35]. On the other hand, researches on THz-induced LIPSS on chalcogenides have been limited to our groups on GST [25,27], and further studies are required to understand their properties. Especially, while Refs. [25,27] focused on the LIPSS parallel to the electromagnetic wave polarization, those perpendicular to the polarization have yet to be analyzed. Since many researches on optically induced LIPSS target both the structures directed parallel and perpendicular to the polarization, investigations on THz-induced LIPSS with both directions are needed for the comparative study with the optically induced LIPSS.

In this work, we analyzed in detail the THz-induced LIPSS on GST samples with the help of Fourier transformation. Two types of LIPSS were observed: one with a larger period, aligned parallel to the THz wave polarization, and another with a finer period, oriented perpendicular to the polarization. These properties are consistent with the low-spatial-frequency LIPSS (LSFL) and high-spatial-frequency LIPSS (HSFL), respectively. The LIPSS period observed in the present study is generally consistent with the previously reported ones in that the period is λ/n (where n is the material's refractive index).

2 Experiment

To generate powerful THz pulses, we used the THz-FEL located at the Research Laboratory for Quantum Beam Science, SANKEN (Institute of Scientific and Industrial Research), The University of Osaka [36]. This system produces exceptionally strong THz pulses with a macro pulse energy of approximately 40 mJ at a frequency of 4 THz. The THz pulses were generated using a 40-MeV L-band (1.3 GHz) electron linac and a permanent magnet

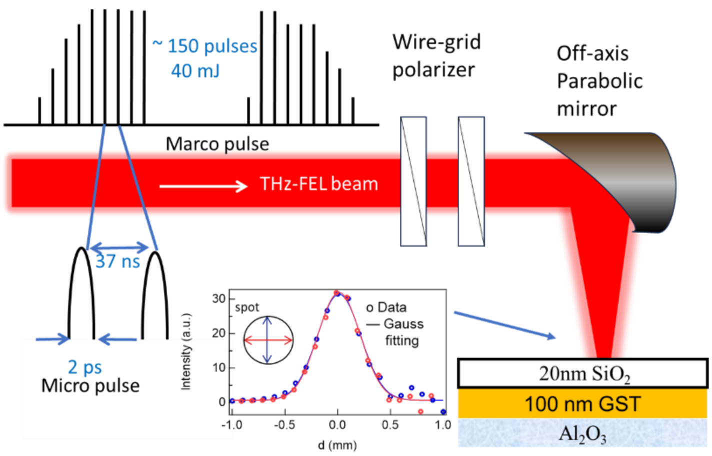

Fig. 1. Schematic diagram of the experimental configuration for THz-FEL irradiation, accompanied by the THz-FEL beam profile measured in two orthogonal directions using the knife-edge method.

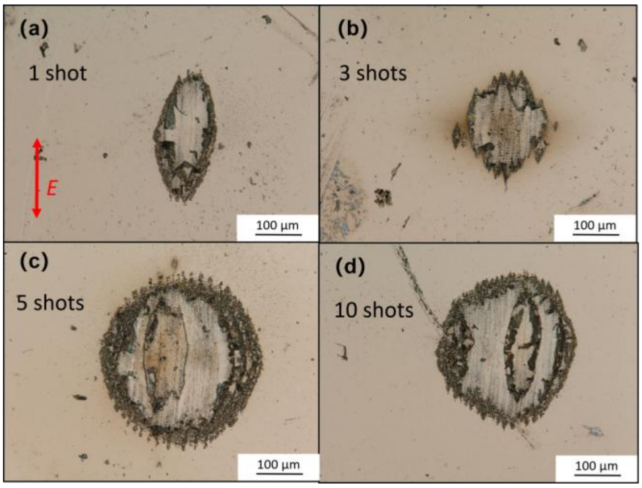

Fig. 2. Microscope images of GST surface after irradiation with (a) 1, (b) 3, (c) 5, and (d) 10 macro pulses of 4-THz FEL beam with 35 J/cm^2 fluence. Red arrow indicates polarization direction.

wiggler. The output frequency was tuned to 4 THz (wavelength 75 µm). The THz macro pulses emitted by the FEL last about 6 µs and consist of approximately 150 micro pulses, with a 37-ns interval between individual micro pulses. Each micro pulse duration is 2 ps. The repetition frequency of the macro pulses was set to 1 Hz. The experimental setup is as shown in Fig. 1, in which the beam is transmitted from a THz-FEL through two metal wire grid polarizers, and the intensity and polarization direction of the beam are controlled. The transmitted beam was focused onto the GST sample surface using a 90° off-axis parabolic mirror with the effective focal length f = 25.4 mm. The focused THz beam profile on the sample surface was evaluated by the knife-edge method with a DLaTGS detector and is shown in the inset of Fig. 1. The fit by a Gauss function shows that the focused spot size at which the intensity becomes 1/e^2 was 0.6 mm both in the direction parallel and perpendicular to the polarization. Because linearly polarized beam was incident perpendicularly onto the GST surface, there is no electric field component perpendicular to the material surface. The maximum energy density of the irradiated area is 35 J/cm^2. The ablation results were investigated using an optical microscope (Keyence VHX6000 or HIROX KH7700). The image observed by the optical microscope was Fourier-transformed to exhibit distinct peaks corresponding to the periodic structures in the LIPSS domain. The position of these peaks reveals the period of the LIPSS, allowing calculation of their spatial period.

For the GST sample, a 100-nm GST thin film was

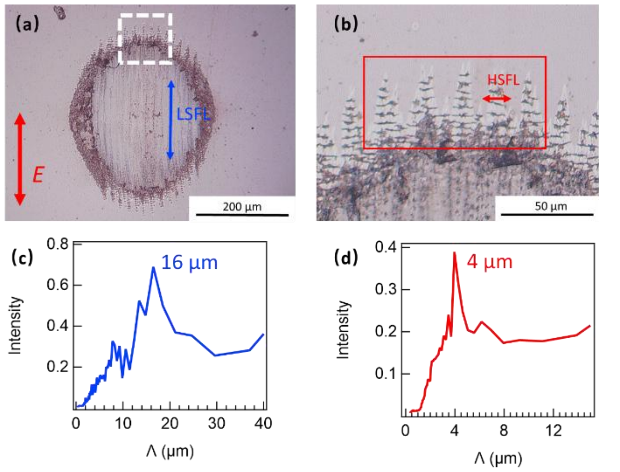

Fig. 3. (a) Microscope image of the GST surface after irradiation with 5 macro pulses of 4 THz FEL beam at a fluence of 14 J/cm^2. (b) Magnified region indicated by the dashed box in (a). (c,d) Period distributions of the structures parallel (c) and perpendicular (d) to the THz wave polarization, obtained by Fourier transform analysis of the red rectangular area in (b). Red arrow indicates polarization direction.

deposited on a 500 µm thick Al_2O_3 substrate by DC magnetron sputtering at room temperature. A stoichiometric $Ge_2Sb_2Te_5$ target was used as the sputtering source. A 20-nm SiO_2 protective layer was deposited on the sample to prevent oxidation. The GST film did not undergo any annealing and thus had an amorphous structure [22].

3 Results

Figures 2(a)–(d) show the microscope images of the GST sample irradiated with 1 to 10 macro pulses of the THz FEL beam at a fluence of 35 J/cm^2. The red arrow in Fig. 2(a) shows the direction of the THz wave polarization *E*. The ablation marks created by 1 shot [Fig. 2(a)] and 3 shots [Fig. 2(b)] were elliptical rather than circular, and while some indications of periodic structures were observed, they were not prominent. After 5 shots, a circular ablation mark with a clear periodic structure was formed [Fig. 2(c)]. The diameter of the mark was approximately 0.4 mm. With additional pulses, the size of the mark did not change significantly, but the central region showed signs of damage by excessive ripple formation and the edges exhibited irregularities caused by multiple exposures [Fig. 2(d)]. This result demonstrates the removal and regeneration process of LIPSS under high-fluence conditions with multiple macro pulse irradiations. To form a clear and stable ablation mark,

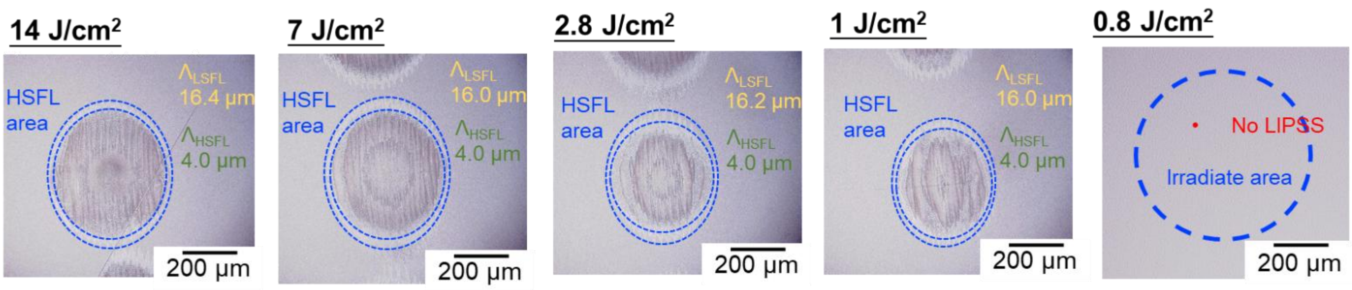

Fig. 4. Fluence dependence of the pattern formed on the GST surface irradiated with 5 shots of 4-THz (75 μm) macro pulses.

we chose 5-shot irradiation in the following experiments. It is also important to note that our previous study [25] showed that THz-FEL irradiation did not induce LIPSS formation on a 20-nm SiO_2 protective layer. Considering the similarly low absorption of SiO_2 in the THz range, LIPSS formation on SiO_2 is also unlikely. We also confirmed that no LIPSS or observable damage was formed on the Al_2O_3 substrates after THz-FEL irradiation. Therefore, we conclude that the observed LIPSS structures are formed in the GST layer rather than in the SiO_2 or Al_2O_3 layers. Direct imaging using scanning electron microscopy (SEM) or transmission electron microscopy (TEM) can reveal the precise spatial distribution of LIPSS within such sandwich-structured materials. Though these methods can provide direct insights into the depth and position of the LIPSS, they require extensive preparation and carry the risk of damaging or losing critical information on the sample. We have to prepare carefully for implementing such cross-sectional characterization as our future work.

Figure 3(a) shows the microscope image of the GST sample after 5 shots. Here we reduced the fluence of the THz beam from 35 J/cm^2 (Fig. 2) to 14 J/cm^2, because the lower fluence was found to result in clearer LIPSS formation. The incident polarization direction E is indicated by the vertical red arrow. In the figure, we can clearly see the formation of periodic ripples parallel to the polarization direction, which extend to the edges, forming a serrated structure. When we magnified and observed the surrounding serrated structures, another periodic structure perpendicular to the polarization direction was observed [Fig. 3(b)].

According to previous reports, the LIPSS with larger period (LSFL) and smaller period (HSFL) typically form parallel and perpendicular to the polarization direction, respectively, when the photon energy of the incident laser is lower than the semiconductor bandgap [3]. In this study, the photon energy of the THz wave used (17 meV) is much lower compared to the bandgap of GST which is approximately 0.7 eV (with slight variations depending on the exact composition and phase, either amorphous or crystalline) [37]. Since this tendency is consistent with our results, hereafter we call the observed periodic structures directed parallel and perpendicular to the THz wave polarization LSFL and HSFL, respectively.

To evaluate the period of these LIPSS, we performed a Fourier transform to the region enclosed by the red rectangle in Fig. 3(b) along the horizontal and vertical directions. This analysis yielded the period distributions of the structures aligned parallel (LSFL) and perpendicular (HSFL) to the polarization as shown in Fig. 3(c) and (d), respectively. The period distribution of the LSFL [Fig. 3(c)] has a peak at $\Lambda_{\mathrm{LSFL}} = 16\ \mu\mathrm{m}$, which is about 1/4.5 of the incident wavelength $\lambda_{\mathrm{THz\text{-}FEL}} = 75\ \mu\mathrm{m}$. On the other hand, the period distribution of the HSFL has a peak at $\Lambda_{\mathrm{HSFL}} = 4\ \mu\mathrm{m}$, which is about 1/18 of the incident wavelength.

According to existing theory, LSFL structures have periods close to λ/n, provided that the photon energy of the light is smaller than the material's bandgap, referred to as the "LSFL-II" pattern [3]. The refractive index of amorphous GST in the THz range was around 4.5 [28]. This result is consistent with our predicted period of λ/n.

To further investigate the characteristics of THz-induced LIPSS on the GST sample, next we observed the dependence of the formed patterns on the fluence of the THz waves (Fig. 4). The periods of both the LSFL and HSFL were almost independent of the fluence. As the fluence was decreased from 14 J/cm^2 to 1 J/cm^2, the area where LIPSS forms became smaller. Accordingly, the annular area where HSFL appeared got smaller and consistently remained at the edges of the formed pattern. As observed in Figure 4, the suppression of LIPSS formation results from the Gaussian fluence distribution of the laser beam, where excessive material removal occurs at high fluences. At 14 J/cm^2, the absence of LIPSS structures in the central region is attributed to the Gaussian energy distribution of the THz-

FEL pulse. The excessively high laser power at the center leads to excessive heat accumulation, causing the material surface to melt and resolidify, effectively erasing any pre-formed LIPSS structures. As the fluence decreases, the thermal effects become less dominant, allowing LIPSS structures in the central region to become progressively clearer.

4 Discussion

4.1 Effect of the SiO_2 layer on LSFL period

In Ref. [38] Derrien *et al.* reported that the period of the LSFL induced by an optical pulse on silicon was significantly reduced in water compared to air, suggesting that the surrounding medium has an effect on the LSFL period. On the other hand, the LSFL period in our sample is close to the theoretically predicted value despite the presence of an SiO_2 layer covering the GST layer. This contrast may be ascribed to the difference in the LSFL formation mechanism. The LSFL in Ref. [38] is perpendicular to the electric field polarization, which indicates that this falls into LSFL-I regime and related to SPP excitation [3]. In this regime, the surrounding medium is expected to strongly influence the LSFL period because the SPP coupling is affected by the surrounding medium. On the other hand, the LSFL observed in our study is parallel to the electric field polarization and categorized into LSFL-II. The formation mechanism of LSFL-II is considered to be related to an effect called radiation remnant, which differs from the mechanism responsible for LSFL-I [3]. Though it is not possible to experimentally confirm the period of LSFL on GST without SiO_2 due to its easily-oxidizable nature, the effect of SiO_2 layer on LSFL period is considered to be smaller than in the case of LSFL-I reported in [38].

4.2 Formation mechanism of the observed LIPSS morphology

We consider that the observed morphologies of the inner LSFL and outer HSFL are formed through a mechanism similar to those reported on LIPSS generated by optical pulses [39,40]: the HSFL structures are formed first due to the interference between the incident field and the scattered near-field below the surface. Subsequently, the interference between the field scattered from the HSFL and the incident field induces transition from HSFL to LSFL-II after the multiple pulse irradiation. Due to the Gaussian profile of the THz beam, the transition does not proceed sufficiently on the outer side of the irradiated spot, resulting in an annular HSFL structure. A distinctive feature of our observed results is the formation of a clear LSFL structure even at a fluence just above the LIPSS formation threshold (1 J/cm^2 in Fig.4) with only 5-shot irradiation. This can be explained by the unique structure of the THz-FEL pulse. As described above, one macro pulse from the THz-FEL contains 150 micro pulses, with a 37-ns interval corresponding to 27 MHz. This irradiation of a large number of pulses with high repetitive frequency will promote the transition from HSFL to LSFL-II more strongly than in the case of optical laser pulse irradiation. Therefore, at fluence levels exceeding the HSFL formation threshold, the central part of the beam reaches the LSFL transition threshold, resulting in the observed morphology where LSFL is surrounded by HSFL.

Compared to previous studies [25,27], this work provides new insights into LIPSS formation under THz-FEL irradiation, distinguishing it from earlier findings. Unlike conventional ultrafast laser-induced LIPSS, our results demonstrate fluence-dependent transitions between LSFL-II and HSFL, influenced by multi-pulse effects and sub-bandgap excitation mechanisms. Notably, we find that HSFL structures are erased at high fluences, confining their formation to the edges of the irradiated region. These results offer a deeper understanding of energy-dependent surface structuring in the THz regime, further advancing research on long-wavelength LIPSS mechanisms.

5 Summary

In summary, we demonstrated the formation of two types of LIPSS on amorphous GST irradiated by a THz-FEL. The first is LSFL, with a period of $\Lambda_{LSFL} \approx \lambda_{THz\text{-}FEL}/4.5$, oriented parallel to the laser polarization. The second is HSFL, which forms at the edge of the ablation marks, with a period of $\Lambda_{HSFL} \approx \lambda_{THz\text{-}FEL}/18$ and an orientation perpendicular to the laser polarization. The period of the LSFL was found to be consistent with what is expected from the "LSFL-II" type proposed in the theory of optically induced LIPSS. We also found that the HSFL always appeared annularly around the boundary of the LSFL-formed area and non-ablated area. Building on our previous work, we successfully generated both LSFL-II and HSFL on THz transparent amorphous GST. LSFL-II and HSFL are quantitatively distinguished through spatial frequency analysis and explain the mechanism behind both LSFL-II and HSFL formation. Our research suggests that when GST is under THz-FEL irradiation, LIPSS formation is primarily a surface-driven process influenced by energy deposition, surface modifications, and multi-pulse effects. The observed HSFL localization at the edges can be explained by the characteristic structure of the THz-FEL output pulse, which consists of micro pulses. This suggests that the morphology where LSFL is surrounded by HSFL is a result of the specific energy deposition dynamics under THz-FEL irradiation. We expect that the unique characteristics of THz-induced LIPSS presented in this work motivate further investigations on LIPSS formation mechanism not only in the THz region but also in the optical region.

Acknowledgment

We thank K. Furukawa and Y. Fukui for their assistance with FEL operation. This work was performed using the THz-FEL based on the L-band electron linac at the Research Laboratory for Quantum Beam Science, SANKEN (Institute of Scientific and Industrial Research), Osaka University. We also thank Prof. M. Nagai of Osaka University for the optical microscopy measurements.

Funding

This work was supported by JSPS KAKENHI Grant Numbers JP24H00317, JP23K17748, JP24H02232. and JST SPRING, Grant Number JPMJSP2138.

Declarations

Conflict of interest The authors declare no conflict of interest.

Contributions

Conceptualization: [M. N], [Y. W. W]; Experiment and investigation: [Y. W. W], [Z. Y], [K. K]; Data analysis: [Y. W. W], [K. K]; Writing-original draft preparation: [Y. W. W]; Writing-review and editing: [K. K], [V. C. A], [T. N. K. P]; GST fabrication: [K. M], [J. T]; THz-FEL management and operation: [G. I]; Funding acquisition and Supervision: [M. N]; Writing-review and editing: All authors.

Data Availability

The data supporting the findings of this study are available from the corresponding author, Makoto Nakajima, upon reasonable request.

Reference

1. M. Birnbaum, Semiconductor surface damage produced by ruby lasers. *J. Appl. Phys.* **36**(11), 3688–3689 (1965).
2. J.E. Sipe, J.F. Young, J.S. Preston, H.M. van Driel, Mechanisms of laser-induced periodic surface structure. *Phys. Rev. B* **27**, 1141 (1983).
3. J. Bonse, S. Hohm, S. V. Kirner, A. Rosenfeld, and J. Kruger*, IEEE J. Sel. Top. Quantum Electron.* **23**, 9000615 (2017).
4. O. Varlamova, J. Reif, Evolution of Femtosecond Laser Induced Surface Structures at Low Number of Pulses near the Ablation Threshold. *J. Laser Micro/Nanoeng.* **8**, 300 (2013).
5. A.Y. Vorobyev, C. Guo, Direct femtosecond laser surface nano/microstructuring and its applications. *Laser Photon. Rev.***7**, 385 (2012).
6. S. Höhm, M. Herzlieb, A. Rosenfeld, J. Krüger, J. Bonse, Formation of laser-induced periodic surface structures on fused silica upon two-color double-pulse irradiation. *Appl. Phys. Lett.* **103**(25), 254101 (2013).
7. S. Höhm, A. Rosenfeld, J. Krüger, J. Bonse, Femtosecond laser-induced periodic surface structures on silica. *J. Appl. Phys.* **112**(1), 014901 (2013).
8. X. Wang, C. Li, C. Ma, J. Feng, W. Hong, Z. Zhang, Formation of laser-induced periodic structures on stainless steel using multi-burst picosecond pulses. *Opt. Express* **26**, 6325–6330 (2018).
9. E. Rebollar, M. Castillejo, T.A. Ezquerra, Laser-induced periodic surface structures on polymer films: From fundamentals to applications. Eur. Polym. J. **73**, 162–174 (2015).
10. R. Buividas, M. Mikutis, S. Juodkazis, Surface and bulk structuring of materials by ripples with long and short laser pulses: Recent advances. *Prog. Quantum Electron.* **38**, 119–156 (2014).
11. F. Müller, C. Kunz, S. Gräf, Bio-inspired functional surfaces based on laser-induced periodic surface structures. *Materials* **9**, 476 (2016).
12. J. Bonse, S. Gräf, Maxwell Meets Marangoni—A Review of Theories on Laser-Induced Periodic Surface Structures.. *Laser Photonics Rev.* **14**, 2000215 (2020).
13. E.L. Gurevich, S.V. Gurevich, Laser induced periodic surface structures

induced by surface plasmons coupled via roughness. *Appl. Surf. Sci.* **302**, 118–123 (2014).

14. L. Khosravi Khorashad, A. Reicks, A. Erickson, J.E. Shield, D. Alexander, A. Laraoui, G. Gogos, C. Zuhlke, C. Argyropoulos, Unraveling the formation dynamics of metallic femtosecond laser induced periodic surface structures. *Opt. Laser Technol.* **171**, 110410 (2024).
15. Y. Fuentes-Edfuf, J.A. Sánchez-Gil, C. Florian, V. Giannini, J. Solis, J. Siegel, Surface plasmon polaritons on rough metal surfaces: Role in the formation of laser-induced periodic surface structures. *ACS Omega* **4**(4), 6939–6946 (2019).
16. L. Gemini, M. Hashida, T. Nishii, Y. Miyasaka, S. Inoue, J. Limpouch, T. Mocek, S. Sakabe, Formation of laser-induced periodic surface structures (LIPSS) on Ti upon double fs pulse exposure. *Proc. SPIE* **9351**, 935117 (2015).
17. M. Hashida, Y. Furukawa, S. Inoue, S. Sakabe, S. Masuno, M. Kusaba, H. Sakagami, M. Tsukamoto, Uniform LIPSS on titanium irradiated by two-color double-pulse beam of femtosecond laser. *J. Laser Appl.* **32**(2), 022054 (2020).
18. J. Bonse, J. Krüger, Pulse number dependence of laser-induced periodic surface structures for femtosecond laser irradiation of silicon. *J. Appl. Phys.* **108**, 034903 (2010).
19. T. Shinonaga, M. Tsukamoto, G. Miyaji, Periodic nanostructures on titanium dioxide film produced using femtosecond laser with wavelengths of 388 nm and 775 nm. *Opt. Express* **22**, 14696 (2014).
20. J. Wang, W. Cai, W. Lu, S. Lu, E. Kano, V. C. Agulto, B. Sarkar, H. Watanabe, N. Ikarashi, T. Iwamoto, M. Nakajima, Y. Honda, H. Amano, Observation of 2D-magnesium-intercalated gallium nitride superlattices, *Nature* **631**, 67–72 (2024).
21. V. C. Agulto, T. Iwamoto, H. Kitahara, K. Toya, V. K. Mag-usara, M. Imanishi, Y. Mori, M. Yoshimura, M. Nakajima, Terahertz time-domain ellipsometry with high precision for the evaluation of GaN crystals with carrier densities up to 10^{20} cm^{-3}, Sci. Rep. 11, 18129 (2021).
22. T. N. K. Phan, T. Shimizu, Y. W. Wang, K. Kato, V. C. Agulto, G. Isoyama, S. Fujioka, M. Nakajima, Third harmonic generation due to free carrier in InSb using a terahertz free electron laser. Opt. Lett. 49, 1073–1076 (2024).
23. T. N. K. Phan, Y. W. Wang, T. Shimizu, K. Kato, V. C. Agulto, G. Isoyama, S. Fujioka, M. Nakajima, Complex anisotropy ratio of third harmonic generation in a semiconductor using a terahertz free electron laser. *Opt. Lett.* **49**, 5039–5042 (2024).
24. T. Kurihara, K. Hirota, H. Qiu, K. T. N. Phan, K. Kato, G. Isoyama, M. Nakajima, Reconfiguration of magnetic domain structures of $ErFeO_3$ by intense terahertz free electron laser pulses. *Sci. Rep.* **10**, 7321 (2020).
25. K. Makino, K. Kato, K. Takano, Y. Saito, J. Tominaga, T. Nakano, G. Isoyama, M. Nakajima, Significant volume expansion as a precursor to ablation and micropattern formation in phase change material induced by intense terahertz pulses. *Sci. Rep.* **8**, 2914 (2018).
26. A. Irizawa, S. Suga, T. Nagashima, A. Higashiya, M. Hashida, S. Sakabe, Laser-induced fine structures on silicon exposed to THz-FEL. *Appl. Phys. Lett.* **111**(25), 251602 (2017).
27. Y. W. Wang, S. Segawa, T. Shimizu, V. C. Agulto, V. K. Mag-usara, K. Kato, K. Miyamoto, T. Omatsu, K. Makino, J. Tominaga, G. Isoyama, M. Asakawa, M. Nakajima, Ablation phenomena by intense terahertz vortex beam. *Appl. Phys. A* **128**, 836 (2022).
28. M.B. Agranat, O.V. Chefonov, A.V. Ovchinnikov, S.I. Ashitkov, V.E. Fortov, Damage in a thin metal film by high-power terahertz radiation. *Phys. Rev. Lett.* **120**, 085704 (2018).
29. K. Makino, K. Kato, Y. Saito, P. Fons, A. V. Kolobov, J. Tominaga, T. Nakano, M. Nakajima, Terahertz generation measurements of multilayered GeTe–Sb_2Te_3 phase change materials, Opt. Lett. 44, 1355–1358 (2019).
30. K. Makino, S. Kuromiya, K. Takano, K. Kato, M. Nakajima, Y. Saito, J. Tominaga, H. Iida, M. Kinoshita, T. Nakano, THz Pulse Detection by Multilayered GeTe/Sb_2Te_3, *ACS Appl. Mater. Interfaces* **8** (47), 32408–32413 (2016).
31. C. Ruiz de Galarreta, S. G.-C. Carrillo, Y.-Y. Au, E. Gemo, L. Trimby, J. Shields, E. Humphreys, J. Faneca, L. Cai, A. Baldycheva, et al., Tunable optical metasurfaces enabled by chalcogenide phase-change materials: from the visible to the THz, J. Opt. **22**, 11 (2020).
32. F. Rao, Z. Song, Y. Cheng, M. Xia, K. Ren, L. Wu, B. Liu, S. Feng, Investigation of changes in band gap and density of localized states on phase transition for $Ge_2Sb_2Te_5$ and $Si_{3.5}Sb_2Te_3$ materials, *Acta Mater.* **60**(1), 323–328 (2012).
33. Y. Katsumata, T. Morita, Y. Morimoto, T. Shintani, T. Saiki, Self-organization of a periodic structure between amorphous and crystalline phases in a GeTe thin film induced by femtosecond laser pulse amorphization. *Appl. Phys. Lett.* **105**, 031907 (2014).
34. Y. Fuentes-Edfuf, M. Garcia-Lechuga, D. Puerto, C. Florian, A. Garcia-Leis, S. Sanchez-Cortes, J. Solis, J. Siegel, Coherent scatter-controlled phase-change grating structures in silicon using femtosecond laser pulses. *Sci. Rep.* **7**, 4594 (2017).
35. Y. Li, V.A. Stoica, L. Endicott, G. Wang, H. Sun, K.P. Pipe, C. Uher, R. Clarke, Femtosecond laser-induced nanostructure formation in Sb_2Te_3. *Appl. Phys. Lett.* **99**, 121903 (2011).
36. K. Kawase, M. Nagai, K. Furukawa, M. Fujimoto, R. Kato, Y. Honda, G. Isoyama, Extremely high-intensity operation of a THz free-electron laser using an electron beam with a higher bunch charge. *Nucl. Instrum. Meth. A* **960**, 163582 (2020).
37. B.-S. Lee, J.R. Abelson, S.G. Bishop, D.-H. Kang, B.-K. Cheong, K.-B. Kim, Investigation of the optical and electronic properties of phase change material in its amorphous, cubic, and hexagonal phases. *J. Appl.*

Phys. **97**(9), 093509 (2005).

38. T. J.-Y. Derrien, R. Koter, J. Krüger, S. Höhm, A. Rosenfeld, J. Bonse, Plasmonic formation mechanism of periodic 100-nm-structures upon femtosecond laser irradiation of silicon in water. *J. Appl. Phys.* **116**(7), 074902 (2014).
39. A. Rudenko, J.-P. Colombier, S. Höhm, M.E. Holz, T.J. Arnold, "Spontaneous periodic ordering on the surface and in the bulk of dielectrics irradiated by ultrafast laser: a shared electromagnetic origin." *Sci. Rep.* **7**, 12306 (2017).
40. C. Florian, J.-L. Déziel, S.V. Kirner, J. Siegel, and J. Bonse, " The Role of the Laser-Induced Oxide Layer in the Formation of Laser-Induced Periodic Surface Structures" *Nanomaterials* **10**(1), 147 (2020).